European Journal of Environmental and Civil Engineering

ISSN: 1964-8189 (Print) 2116-7214 (Online) Journal homepage: https://www.tandfonline.com/loi/tece20

Analysis of the fabric of undisturbed and pluviated silty sand under load over time

Muhamad Yusa, Elisabeth T. Bowman & Misko Cubrinovski

To cite this article: Muhamad Yusa, Elisabeth T. Bowman & Misko Cubrinovski (2019): Analysis of the fabric of undisturbed and pluviated silty sand under load over time, European Journal of Environmental and Civil Engineering, DOI: 10.1080/19648189.2018.1541825

To link to this article: https://doi.org/10.1080/19648189.2018.1541825

EUROPEAN JOURNAL OF ENVIRONMENTAL AND CIVIL ENGINEERING
https://doi.org/10.1080/19648189.2018.1541825

Analysis of the fabric of undisturbed and pluviated silty sand under load over time

Muhamad Yusa[a], Elisabeth T. Bowman[b] and Misko Cubrinovski[c]

[a]Civil Engineering Department, University of Riau, Pekanbaru, Indonesia; [b]Civil and Structural Engineering Department, University of Sheffield, Sheffield, United Kingdom; [c]Civil and Natural Resources Engineering Department, University of Canterbury, Christchurch, New Zealand

ABSTRACT

Microstructure of two undisturbed silty sands with 4% fines and 35% fines is described and quantified. The materials were sampled by the gel push sampling method. Upon reloading to their *in situ* stresses, the material fabric was fixed by resin impregnation. A qualitative and quantitative comparison of the microstructure was made with laboratory prepared dry deposited specimens (15% fines) which were loaded over different periods of time. The microstructure is quantified statistically by measuring particle orientation and the distribution of spatial distance between particles. Both undisturbed and reconstituted specimens show a preferred horizontal particle orientation, with little detectable change over time in the reconstituted samples. Spatial microstructural change was assessed using new parameter called index of dispersion. A greater index of dispersion suggests a more interlocked structure (hence, more structurally stable sample). Analysis of the reconstituted samples show that index of dispersion tends to increase with ageing, with the denser sample displaying greater change over time than the looser sample. Values of index of dispersion of reconstituted samples (15% fines) tend to lie between those of the undisturbed sample with 35% silt fines and with 5% fines, showing that this measure is not independent of the particle size distribution.

ARTICLE HISTORY
Received 3 March 2018
Accepted 22 October 2018

KEYWORDS
Microstructure; apparent particle orientation; spatial distance; silty sand; undisturbed; dry deposition

Introduction

Granular disturbed soils exhibit time-dependent behaviour regardless of their near-instantaneous pore water dissipation and chemically hard inert properties. The majority of this evidence comes from the increase in penetration resistance in hydraulically placed fills and freshly disturbed deposits after ground improvement, such as via explosive blasting and dynamic deep compaction (Ashford, Rollins, & Lane, 2004; Saftner, 2009). This phenomenon usually is referred as sand ageing. Another phenomenon related to sand ageing is the increase in pile capacity of driven piles in sands (Bullock, Schmertmann, McVay, &Towsend, 2005; Ng, Selamat, & Choong, 2010). Ageing is particularly important to the behaviour of shallow soils after artificial deposition or disturbance and the time-dependent development of shear resistance after seismic liquefaction.

It is well known that the microstructure of granular soil has a profound influence on its mechanical behaviour. Particle orientation and arrangement of the contacts between grains are the

CONTACT Muhamad Yusa m.yusa@eng.unri.ac.id Civil Engineering Department, University of Riau, Jl HR Subrantas Km 12.5, Pekanbaru 28293, Indonesia.

most important microstructural characteristics to affect stress-strain behaviour (Kang, Yun, Lau, & Wang, 2012; Oda & Iwashita, 1999). Different methods of preparation of reconstituted granular soils have been found to result in a different microstructure and consequently different mechanical response (Hoeg, Dyvik, & Sandbaekken, 2000; Yamamuro, Wood, & Lade, 2008). However, the majority of the microstructure studies were conducted on clean sand, whilst most granular materials occurring in nature are composed of a broad range of particle sizes (Astedt, Weiner, & Holm, 1992; Mitchell & Soga, 2005). Furthermore, very limited microstructure studies are related to ageing of sand with fines.

This research describes an experimental approach to obtain detailed observations of soil microstructure from resin injected granular soils. The experimental techniques can be applied to soils of a relatively wide grain size distribution, and here we focus on their application to silty sands. We provide observations and quantitative measurements of fabric of two undisturbed soils, one fine sand with relatively low silt content and one with high silt content, obtained using a gel push sampler (Taylor, Cubrinovski, & Haycock, 2012). Extending from a preliminary study (Yusa, Bowman, & Cubrinovski, 2017) the particular focus here is on understanding how we can examine and quantitatively compare the fabric of soils of different particle size. These fabric features are then compared with fabric developed in laboratory tests on reconstituted silty sand samples over time under constant stress loading. Here, we examine whether we can detect ageing effects in silty sand.

Material and experimental procedure

Material

Natural undisturbed soil samples were recovered using the gel-push sampling technology (Huang, Tai, Lee, & Ishihara, 2008; Kazuo & Kaneko, 2006). Following the Canterbury earthquake sequence 2010–2011, the method was brought to New Zealand as part of a research project on liquefaction assessment within the Christchurch area (Stringer, Cubrinovski, & Haycock, 2016). The samples were obtained in August 2011 from two sites within the Christchurch Business District (CBD), that is, Kilmore Street (Gel Push-A) and Madras Street (Gel Push-B), that were liquefied by the Mw 6.3 earthquake that occurred in February 2011 (Cubrinovski, 2013; Cubrinovski et al., 2011). Samples Gel Push-A and Gel Push-B were taken approximately from 6 and 4 m depth, respectively. Careful handling of the sample during the gel-push operations and transportation to the laboratory is essential for minimising disturbance. After extrusion of the sample from the tube, the samples are cut and stored, and then trimmed to about 40 mm in height and 50 cm in diameter. The particle size distributions (PSD) obtained by laser sizer are

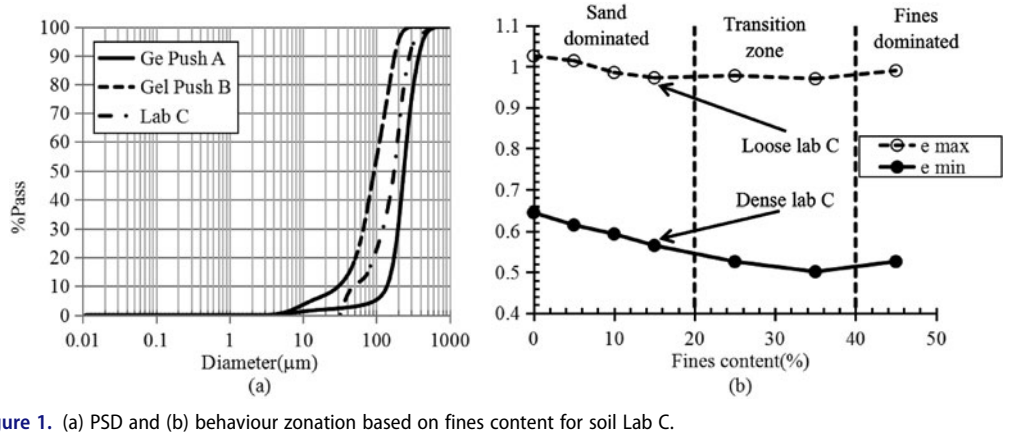

Figure 1. (a) PSD and (b) behaviour zonation based on fines content for soil Lab C.

shown in Figure 1(a). Gel Push-A was a relatively clean sand with 4% fine particles (smaller than 75 μm), while Gel Push-B was a silty sand with 35% fines. The mean diameter D_{50} of Gel Push-A and Gel Push-B was 235 and 95 μm, respectively. The coefficient of uniformity C_u of Gel Push-A and Gel Push-B was 1.7 and 3.7, respectively.

Lab C was ejected soil following the Canterbury earthquake, collected from Rydal Reserve, Christchurch, New Zealand. Lab C is a non-plastic silty sand with 15% fines, mean diameter of 150 μm and coefficient of uniformity of 4.1. For Lab C only, fines particles smaller than 32 μm were removed by wet sieve to avoid difficulty in precise fabric quantification in related work. The maximum and minimum void ratio emax and emin for Lab C were determined as 0.973 and 0.565, respectively, according to the Japanese Geotechnical Society (2009). Lab C specimens were reconstituted by dry funnel deposition (Yamamuro & Wood, 2004). Although size segregation can occur during dry deposition, segregation also generally occurs in the field. Thus for this study, we considered the method is reasonable to make qualitative and quantitative comparison between the microstructure of the natural undisturbed soil and reconstituted soil, and to examine if short-term changes in microstructure of the soil under K_0 loading could be detected by image analysis.

To illustrate the influence of fines content on the maximum and minimum void ratio achievable for Lab C silty sand, Figure 1(b) presents data for a range of sand-fines mixtures. At 15% fines content, the soil is sand dominated – that is, the fines do not participate in the sand matrix and are generally able to move freely between them. As the fines content increases, the fines increasingly fill the voids and, through the transition zone, act to separate the sand particles, resulting in a decrease of emin, followed by an increase as fines begin to dominate the soil's matrix. Although the transition zone is not distinct in the figure, it is taken to be within the range of 20–40% as found by other researchers (Cubrinovski & Ishihara, 2002; Lade, Liggio, & Yamamuro, 1998). Assuming similar soil characteristics, Gel Push-A is expected to be highly sand dominated, while Gel Push-B is in the transition zone although close to being fines dominated.

Experimental procedure

Sample preparation

Microstructure studies can be undertaken by direct methods, for example, injection of a low viscosity epoxy resin to fix the soil particles in place, then sectioning (Palmer & Barton, 1986) or non-direct methods, such as use of X-ray tomography (Vlahinić, Andò, Viggiani, & Andrade, 2014). Reporting on X-ray tomography, Vlahinić et al. (2014) found that, despite the advantage of inducing no disturbance to samples, tomography has limitations with respect to imaging soils that have either wide grain size distribution, irregular shape or fine particles. Hence, it was decided to adopt a direct method of visualisation here.

The setup used for sample preservation by epoxy resin is shown in Figure 2. The epoxy resin used in this study was EPO-THIN from Buehler, Inc., which has specific gravity of 1.1299, viscosity of 200–250 centipoise (cPs) at 20 °C and shrinkage strain of 0.01%. The viscosity of the resin can be reduced to be close to water (1 cPs) when heated to 50 °C for 10 minutes, and has been used in previous research by Masad (1998) and Bowman and Soga (2003). The mixing ratio for the resin and hardener was as recommended by the manufacturer, that is, 5:1.95. The Gel Push-A and Gel Push-B specimens were carefully placed inside the chamber (half split steel cylinder) and dried in the oven under 50 °C for at least two days to achieve full dryness. The maximum axial strain after drying was 0.2%, indicating low disturbance. They were then loaded to 80 and 50 kPa vertical stresses, respectively (Table 1). The vertical stresses were based on the estimated *in situ* stresses corresponding to the sampling depth and groundwater level at the borehole (assuming an average unit weight of 18 kN/m^3). Resin was placed in the upper part of the water epoxy chamber (D) separated from the lower water filled section by a rubber membrane. Pressure was

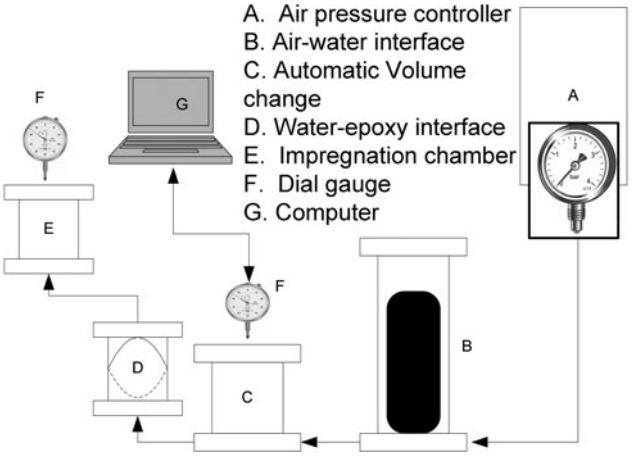

Figure 2. Setup for sample impregnation.

Table 1. Fabric tests conducted.

No	Test ID	Method	Dr (%)	σ'v (kPa)	K_0	Period of constant load
1	Gel Push-A	UD	na	80	na	1 hour
2	Gel Push-B	UD	na	50	na	1 hour
3	Lab C_70601H_DD	DD	70	113	0.53	1 hour
4	Lab C_70601W_DD	DD	70	113	0.53	1 week
5	Lab C_40601H_DD	DD	40	125	0.48	1 hour
6	Lab C_40601W_DD	DD	40	125	0.48	1 week

DD: dry deposition; Dr: relative density; na: not available; UD: undisturbed from gel push sampling.

applied using an air-water interface (B) to inject the resin into the base of the impregnation chamber (E) via the rubber membrane. The air-water interface (B) was connected to an automatic system for volume change (C). In-house software was made to allow monitoring of the resin volume infiltrated. Precaution was taken to ensure air-bubbles were expelled from both sides of the interface chamber. This enabled an accurate assessment of the quantity of resin being used as the infiltration was carried out.

For Lab C, two pairs of samples were reconstituted by dry deposition (Lab C-DD) to a relative density of 40% (loose) and 70% (dense), respectively, making four samples in all. The samples were then loaded one dimensionally under K_0 condition and left for one hour or one week, respectively. This was thought to be sufficient to result in detectable changes in relative microstructure with time (e.g. Bowman & Soga, 2003; Muszynski, 2000). The field stresses under which many soils age may be approximated by the K_0–condition where lateral (horizontal ground) strain is zero. The applied vertical load was in accordance with the K0 value to achieve 60 kPa horizontal effective stress as determined by triaxial testing under K_{00} condition (Yusa & Bowman, 2013). This resulted in applying vertical effective stresses of 113 kPa for the loose and 125 kPa for the dense specimens.

The resin was warmed for 10 minutes at 500 °C to reduce the viscosity. After mixing with the hardener, the epoxy mix then was poured inside the interface chamber and pressurised using an air-water interface to a low pressure to minimise disturbance to the microstructure during injection. The maximum, minimum and average axial strain after the process of injection and curing were 0.3%, 0.0% and 0.15%, respectively, indicating insignificant disturbance. Impregnated samples were then left for 24 hours before being removed from the chamber.

The samples were assumed to be cross anisotropic both with respect to their fabric and stress, with the major principle stress in the vertical direction and minor in the horizontal. Vertical sections were therefore used to capture the fabric in the major and minor principle

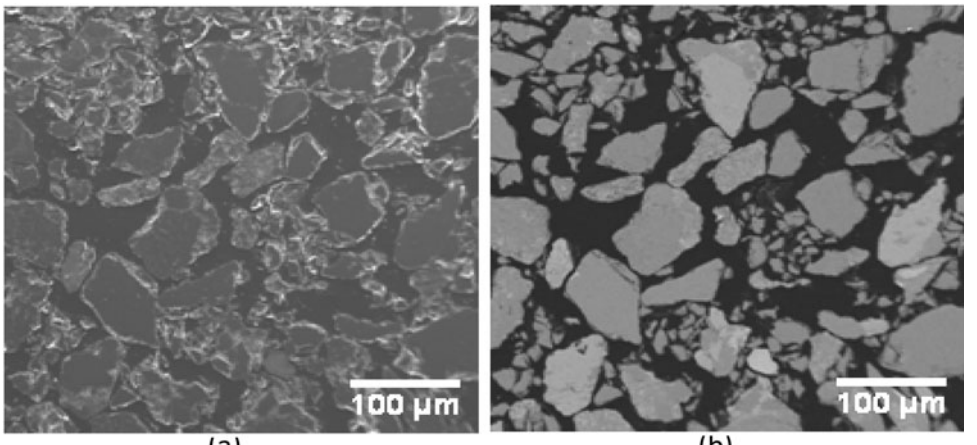

Figure 3. SEM image of the same area, that is, 437 by 437 μm^2 from (a) secondary electron and (b) back scatter mode.

stress directions. Cured samples were cut vertically down the middle of the specimen using a thin 5″ diameter of wavering diamond blade for minimal surface damage. The end result was a thick section of 0.5 cm. Each section was then ground using successive abrasive discs, that is, grit grades 180, 240, 320, 600 and 1200. The section was visually inspected by optical microscope and rotated 90° between steps to remove scratches. From this, no bias in damage to or removal of particular particle sizes could be detected. Finally, the sample was polished using 0.3 μm alpha alumina powder to remove scratches from the finest sandpaper without imparting additional disturbance to the sample.

Capturing image

Scanning electron microscopy (SEM) was used to capture the images, using both secondary electron and back-scattered electron detection modes. Back-scattered detection produces images based on the atomic weight (Lloyd, 1987), giving a clear contrast between the higher atomic weight grains (appearing lighter) and the epoxy filled voids with lower atomic weight. Figure 3 shows image examples of the same area, that is, 211 pixels by 211 pixels equivalent to 437 by 437 μm produced by (a) secondary electron and (b) back-scattered detector modes, captured at 45× magnification. It can be seen that secondary electron mode produces images that contain less detail and are prone to creating confusion between grains and voids, while clearer and more accurate grain edge definition is achieved with greater contrast by use of back scatter mode. Thus, back scatter mode was chosen at a scale resolution of 0.48 pixels/μm. It should be noted that each image or coupon taken represents only a small area of the whole, that is, covering an area of just over a square centimetre. To represent the statistics of each test to a suitable degree, nine images were taken from the left, centre and right, and in three rows, from the top, centre and bottom of each section.

Processing image

Captured images were processed and analysed using image analysis software ImagePro Plus v.7.0. Steps involved in this included contrast enhancement, correction for noise and thresholding. Watershed was then performed to separate the grains automatically. Finally, some manual corrections were made, where necessary, by visual inspection due to imperfections in the watershed process. As the final check, the mean void ratio from the combined images compared with that determined from bulk measurements show a good consistency, for example, for dense

samples (Lab C_70601H_DD and Lab C_70601W_DD) 0.684 and 0.687, respectively, from images compared to 0.686 bulk; for loose samples (LabC_40601H_DD and LabC_40601W_DD) 0.873 and 0.852, respectively, compared to 0.810.

Analysis method

Particle measurement orientation

The orientation of a non-spherical particle can be represented by the orientation of the long axis of the particle relative to a reference axis. The true three-dimensional long axis of the particle is difficult to determine, however a measure of this can be taken from two-dimensional projections. Thus in this study, particle orientation is defined by the angle of the apparent long axis of the projected particle in two dimensions (a vertical plane in this study). The orientation of each particle was determined as the angle between the long axis and the vertical direction and represented on a rose diagram. Statistical parameters were then determined to summarise the distribution of particle orientation using Fisher distribution analysis (Fisher, 1993). The Fisher distribution function PdA(α) gives the normalised probability of finding a unit vector direction within an angular area dA, at angle of α from true mean direction (at which α = 0):

$$P_{dA}(\alpha) = \frac{\kappa}{2\pi \sinh(\kappa)} \exp[\kappa.\cos(\alpha)]\sin(\alpha) \tag{1}$$

where α is the angle between the unit vector and the true direction and κ is a measure of the concentration of the distribution about the true mean direction. The value of κ ranges from zero to infinite. Zero value of κ means that the particle distribution direction is random. When κ approaches infinity the particles are oriented in the same direction.

The properties of particle orientation distribution can be obtained by the resultant vector length (Ψ), mean resultant length (r) and mean angle (α_m) determined using Equations (2) to (4):

$$\Psi^2 = \sqrt{\left\{\sum_{i=1}^{N}[l_i.\sin(2\alpha]\right\}^2 + \left\{\sum_{i=1}^{N}[l_i.\cos(2\alpha]\right\}^2} \tag{2}$$

$$\boldsymbol{r} = \frac{\boldsymbol{\Psi}}{\sum_{\boldsymbol{i=1}}^{\boldsymbol{N}} \boldsymbol{l_i}} \tag{3}$$

$$\alpha_m = \frac{1}{2}\tan^{-1}\left(\left\{\sum_{i=1}^{N}[l_i\sin(2\alpha_i]\right\} / \left\{\sum_{i=1}^{N}[l_i\cos(2\alpha_i]\right\}\right) \tag{4}$$

where l_i is the length of long axes of the particle, N is the number of measurements, α is the angle between the unit vector and the true direction. The value of r ranges from zero to one. Higher r value indicates more orientated data. For number of data >15, κ can be estimated from r as follows (Fisher, 1993):

$$\kappa = \begin{cases} 2r + r^3 + \frac{5}{6}r^5 & ; r < 0.53 \\ -0.4 + 1.9r + \frac{0.43}{1-r} & ; 0.53 \le r < 0.85 \\ \frac{0.43}{1 - 3r^2 + r^3} & ; r \ge 0.85 \end{cases} \tag{5}$$

The influence of different scales of particle structure on the behaviour of soil is unknown. A silty sand with a relatively large number of fines particles, that is, silt dominated, may have different scales of interest from one that is dominated by larger particles. The statistical results of rose

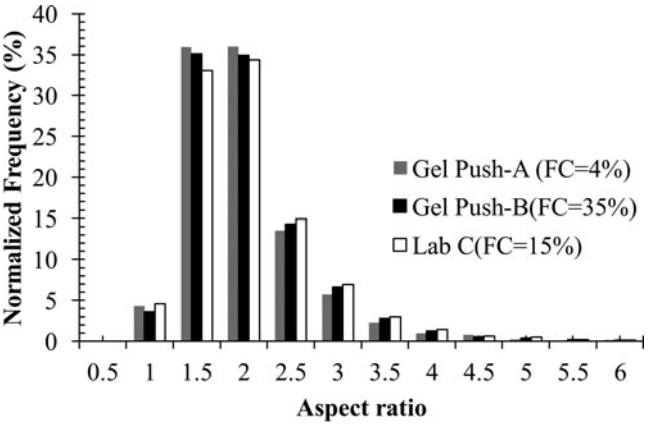

Figure 4. Frequency distribution of aspect ratio.

diagrams in which all fines are included, for example, will be controlled by the fine particles although the large particles may predominantly form the major force columns and govern the soil's mechanical behaviour. Hence, to avoid bias related to particle size, we use a weighted value by grain areas for the orientation of each particle. The weighted rose diagram gives a higher significance to the orientation of larger particles (sand in this study), as described in Yang (2002).

Particle aspect ratio distribution

Particle aspect ratio (AR) is a measure of elongation and is defined as the ratio of the particle's long axis length, dL, to its short axis, dS, as formulated in Equation (6).

$$AR = \frac{dL}{ds} \tag{6}$$

Normalised frequency (frequency in each bin is divided by total number of particles) distribution histograms of aspect ratio is shown in Figure 4. It can be seen that most particles (∼70%) for both Gel Push-A and B have aspect ratio between 1.5 and 2, showing that they are elongated. A similar aspect ratio distribution is seen for Lab C.

Spatial distance statistic

In addition to particle orientation, the spacing or size of local voids between the particles has important influence on soil behaviour. For example, Masad (1998) used the mean free path (distance between grains in a given direction, also known as the mean intercept length) to examine the seepage anisotropy through granular soils, while Kang et al. (2012) shed light on the mechanism of creep by drawing the evolution of void orientation with time. Bowman (2002) thought that interlocking of particles may cause soils to age. The interlocking of particles is related to particle edge proximity, so that a mean free path method was used in that study to measure the distribution of spatial distance between particles. Following the same reasoning, we use the approach here. For the mean free path method, a series of scanning lines is drawn which pass through both solid particles and voids and the lengths of the spacing between solid particles are measured (Kuo, Frost, & Chameau, 1998; Masad & Muhunthan, 2000). The directions of the scanning lines used here were vertical and horizontal, commensurate with principal vertical and radial stresses in axisymmetry. In this study, the shift distance of scan line was set to be small enough (i.e. 10 pixels) so it could pass through the fine particles, hence in one image

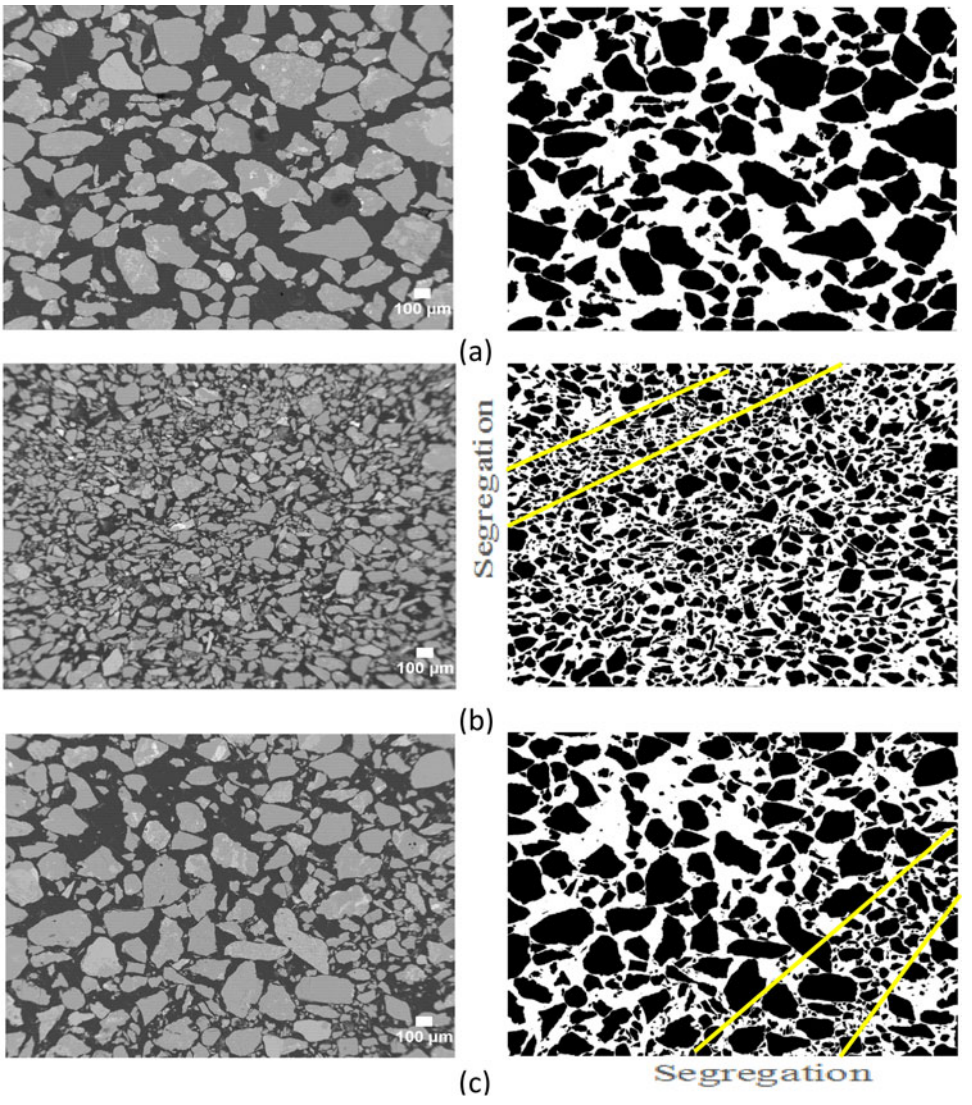

Figure 5. Captured (left) and processed (right) 2650 (wide) × 2120 µm (high) images (a) Gel Push-A, (b) Gel Push-B, and (c) Lab C. Black is solid, white is void.

(1280 × 1024 pixels) the number of lines is 128 in the vertical direction and 102 in the horizontal direction.

The distance between particles as measured along a scan line generally produces a highly skewed distribution with many small gaps and few larger ones. In order to apply meaningful statistics, this type of distribution should be transformed to approach normality (Chatfield, 1983), as previously proposed by Bowman and Soga (2003). Parameters used in this analysis are therefore mean log of void distance, kurtosis of the log of void distance, and the ratio of variance of the log of void distance to the mean log void distance, also known as the index of dispersion. The mean void distance of a sample image is, as expected, somewhat related to the whole sample void ratio. Void ratio of the sample, e, is defined as the volume (or image area) of voids (white area) to that of the solids (black area), as illustrated in Figure 5. Kurtosis is defined as the fourth moment of a probability distribution and is a measure of the shape of a curve. High values of kurtosis can occur where there are large numbers of values concentrated in the extreme tails of

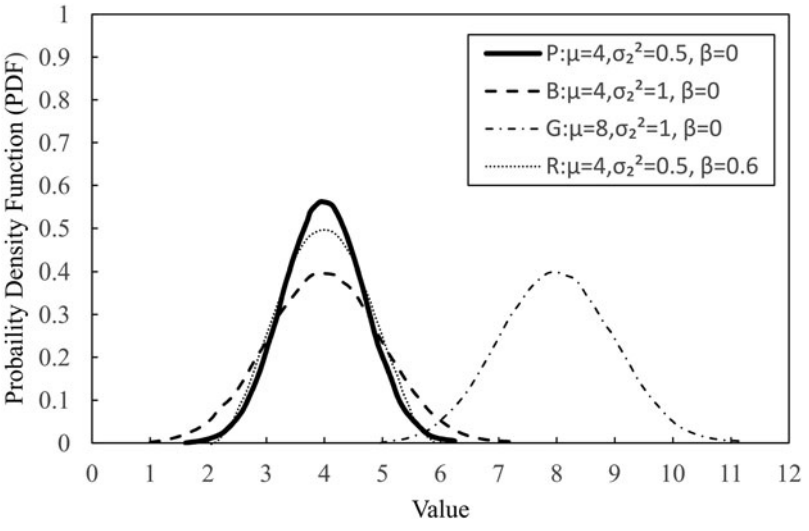

Figure 6. Example probability density functions (PDF) of different distributions with different values of mean, μ, variance, σ^2, and kurtosis, β.

the distribution, with a value of 3 indicating a normal distribution. The excess population kurtosis, β, used here, is defined as kurtosis minus 3, so a value of zero indicates a normal distribution. It is formulated for a sub-set of samples within a population as:

$$\beta = \left[\frac{n(n+1)}{(n-1)(n-2)(n-3)}\sum\left(\frac{x-\mu}{s}\right)^4 - \frac{3(n-1)^2}{(n-2)(n-3)}\right] \tag{7}$$

where x is the log void distance along a scan line, μ is the mean value, n is the number of samples and σ is the standard deviation, defined as:

$$\sigma^2 = \frac{\sum (x-\mu)^2}{n} \tag{8}$$

where σ^2 is also known as the variance. Low (more negative) values of excess population kurtosis β (henceforth simply referred to as 'kurtosis') generally implies 'shoulder-heavy' distributions, while high values indicates greater 'tailness' (Johnson, Tietjen, & Beckman, 1980).

Figure 6 shows this concept generally, using probability density functions of three normal distributions in which β = 0 (Line P, B and G) and one raised cosine distribution (Line R) in which β < 0 at –0.6 (noting that this is just one illustrative non-normal distribution). Increasingly low values of kurtosis of void distribution were considered by Bowman and Soga (2003) to relate to particle interlock with time – that is, the particles would become clustered together, increasing the shoulders of the distribution. In the extreme long term however, it may be that kurtosis values will then increase as a result of void distance distributions entering the extreme tails. For example, in Figure 6, lines P and R and have the same mean and variance, but different kurtosis, with R having a higher (more positive) value. The shoulders of the distribution of R are broader, but the extremes are less – indicating the ambiguity of kurtosis as a true measure of cluster. As a result, a new measure is also introduced here.

The variance to mean ratio (index of dispersion) is a normalised measure of whether a set of data is clustered or dispersed. Comparing lines P and R (as above), the index of dispersion is the same, which seems reasonable as it accounts both for the shoulders and tail of the distribution. It is also useful when comparing populations with different means. In Figure 6, lines G and B have the same variance but for G the mean is higher than for B, so that the index of dispersion is lower. For distributions that have either larger shoulders or tails, relative to the mean, the

index of dispersion should be greater (e.g. B versus all others in Figure 6). Therefore, a higher index of void dispersion is expected to indicate a more interlocked fabric, that is, the soil fabric would contain greater numbers of large and small gaps between the particles for a given mean void ratio, than for a non-interlocked structure. Note that here, we report results on both kurtosis and index of dispersion, in order to examine which may be the most appropriate measure of particle interlock.

Results

Qualitative results

Examples of captured and processed 2650 × 2120 μm images from Gel Push-A, Gel Push-B and Lab C are presented in Figure 5(a–c), respectively. Notable bands of fine particles are visible in this figure for Gel Push-B and for Lab C. Lab C shows a band of silt running from the bottom to the right edge. For Gel Push-B, a band runs from the left edge to the top, showing that particle size segregation occurs naturally in the field as well as in reconstituted dry deposition samples. The typical number of particles in one image is approximately 200, 2000 and 1000 for Gel Push-A, Gel Push-B and Lab C, respectively. With nine images taken per section, statistical analysis involved approximately 1800, 18,000 and 9000 particles for Gel Push-A, Gel Push-B and Lab C, respectively.

Particle orientation and diagrams

Jang (1997), based on extraction of soil by ground freezing, found qualitatively that sands under natural deposition have a preferred orientation towards the horizontal. Here, we present results of quantification of grain orientation for natural deposits of silty sand. Histograms of particle orientations for each test are grouped into 10 degree intervals. Separate analyses for 'sand'-sized and 'fines'-sized particles were also performed in order to see whether there was difference in the orientation anisotropy between large and small grains. It is not possible to determine which particles truly are fines (taken as <75 μm in diameter) due to the fact that a 2D slice through each particle may not occur diametrically. Regardless, it can be determined that particles having a ferret minimum (smallest distance between two parallel tangents) equal to or larger than 75 μm are sand. In this study, the rest of the particles are assumed to be fines. This results in higher fines percentages being reported than those from the true PSD, as shown in Table 2.

It can be seen from Table 3 that the fabric of natural undisturbed sand (Gel Push-A and B) has a preferred apparent orientation to the horizontal with mean angles of 87.8° and 89.1° to the vertical axis, respectively. A similar trend was found for Lab C with dry pluviation. Table 3 also reveals that sand size particles and fines tend both to be horizontally oriented, but that fines are less orientated than sand particles, as indicated by smaller κ values. The latter result is likely to be influenced also by the fact that some particles marked as 'fines' are actually small portions of larger particles. Examination of the reconstituted specimens suggests that the

Table 2. Fines content (<75 μm) from PSD and image analysis.

		Measured fines content (%)	
Test	Description	PSD	Image analysis
Gel Push-A	Undisturbed sample	4	5.4
Gel Push-B	Undisturbed sample	35	52.8
Lab C 40601H _DD	Loose – 1 hour aged	15	20.4
Lab C 40601W _DD	Loose – 1 week aged	15	17.4
Lab C 70601H_DD	Dense – 1 hour aged	15	28.3
Lab C 70601W_DD	Dense – 1 week aged	15	25.5

Table 3. Fischer statistical result.

Sample		$\alpha_m(^\circ)^a$	κ
Gel Push-A	All	87.8 ± 1.2	0.53
	Sand size	88.9 ± 0.9	0.60
	Fines size	81.9 ± 3.0	0.33
Gel Push-B	All	89.1 ± 0.7	0.52
	Sand size	87.3 ± 0.9	0.80
	Fines size	89.1 ± 0.6	0.51
Lab C 40601H _DD	All	86.5 ± 1.1	0.42
	Sand size	86.5 ± 0.8	0.65
	Fines size	87.1 ± 1.3	0.29
Lab C 40601W _DD	All	89.6 ± 0.8	0.40
	Sand size	90.5 ± 0.8	0.68
	Fines size	88.2 ± 1.7	0.25
Lab C 70601H_DD	All	84 ± 0.9	0.36
	Sand size	81.2 ± 0.9	0.63
	Fines size	87.9 ± 1.6	0.24
Lab C 70601W_DD	All	89.1 ± 0.8	0.42
	Sand size	87.5 ± 0.9	0.63
	Fines size	91.5 ± 1.4	0.30

[a]Angle measured from vertical clockwise.

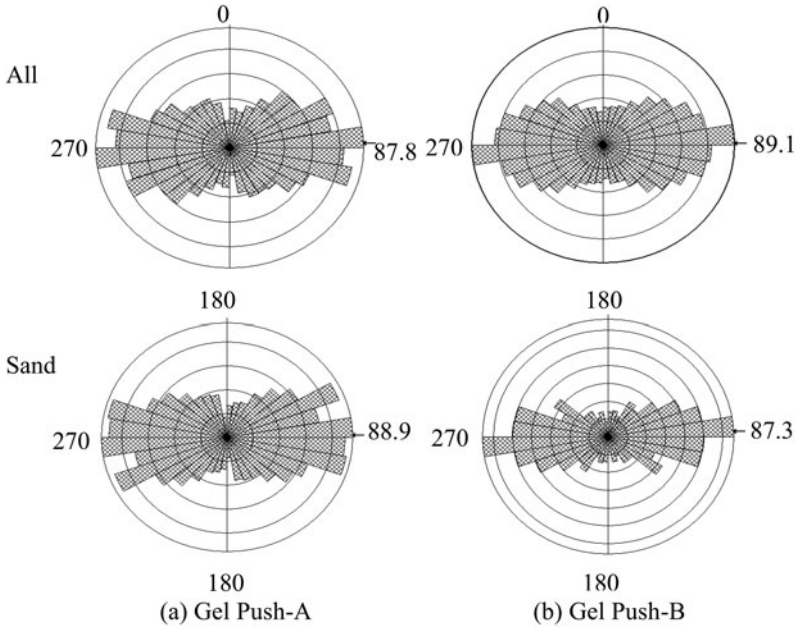

Figure 7. Rose diagram from gel push (a) Gel Push-A and (b) Gel Push-B.

orientation of particles may increase slightly, from an already aligned near-horizontal direction over one week for both dense and loose Lab C samples, while the degree of concentration for all particles tends not to change much.

Rose diagrams for Gel Push-A and B are shown in Figure 7(a,b), respectively and for reconstituted samples are presented in Figures 8 (loose) and 9 (dense). The rose diagrams visually confirm the similarity between natural soils and dry deposition samples in terms of particle orientation.

Spatial distance distribution

In order to carry out a particle spatial distribution analysis, a minimum representative elementary area (REA) is needed for each image. The REA was determined by drawing a circular area which

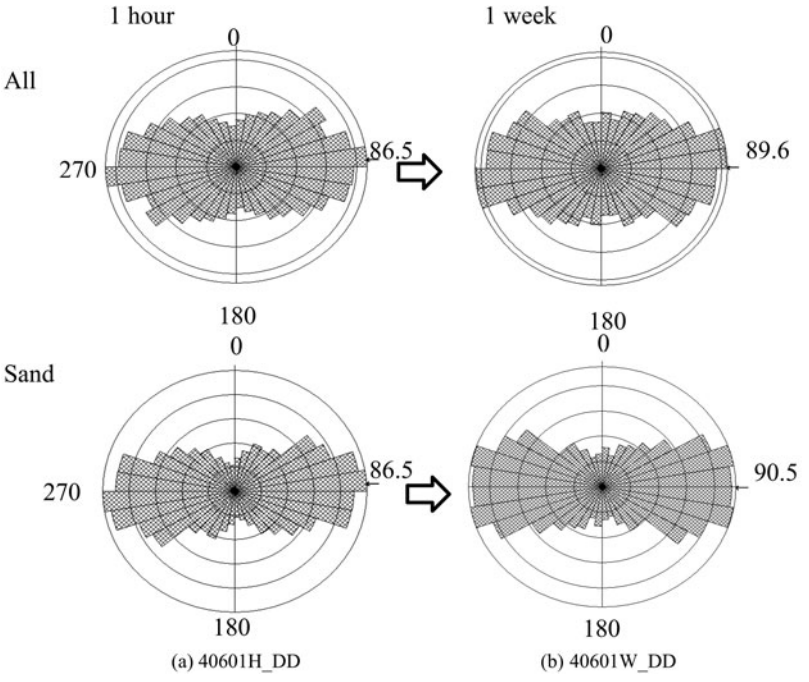

Figure 8. Rose diagram for loose sample (a) 40601H_DDl and (b) 40601W_DD.

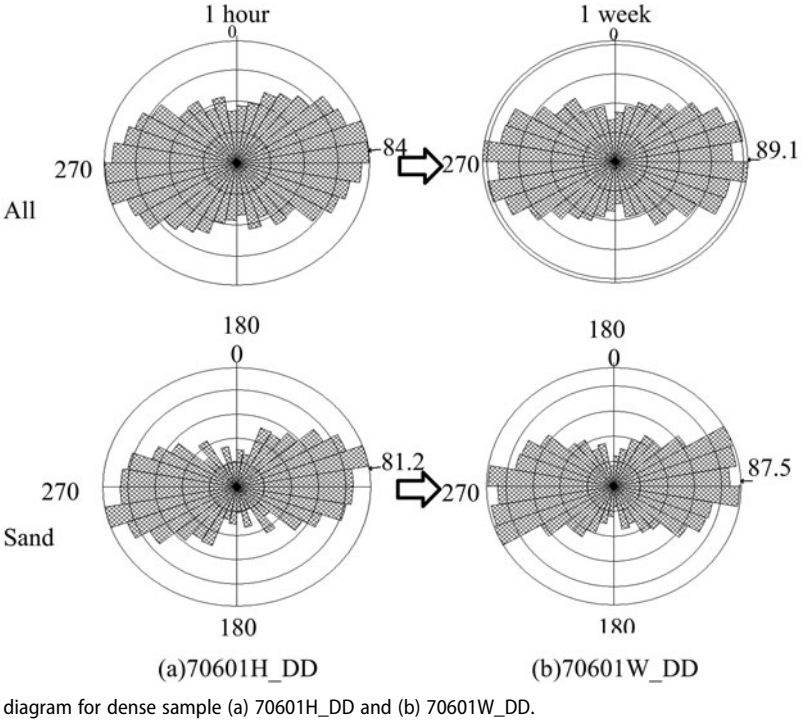

Figure 9. Rose diagram for dense sample (a) 70601H_DD and (b) 70601W_DD.

was progressively enlarged until a constant void ratio was obtained (Yusa, 2015). For example, for Lab C_70601H_DD this occurred at an area of about 900,000 pixels which is equivalent to a REA diameter of 1070 μm.

Table 4. Spatial void distance results for gel push and reconstituted samples.

			Mean log spacing		Kurtosis		Index of dispersion	
Sample	Image 'Fines' content (%)	Void ratio	V	H	V	H	V	H
Gel Push-A	5.4	0.733	1.281	1.325	−0.620	−0.585	0.185	0.188
Gel Push-B	52.8	0.726	0.944	1.028	−0.660	−0.695	0.151	0.157
Lab C (40601H_DD)	20.4	0.873	1.064	1.079	−0.745	−0.770	0.179	0.173
Lab C (40601W_DD)	17.4	0.852	1.051	1.088	−0.787	−0.699	0.186	0.174
Lab C (70601H_DD)	28.3	0.684	1.056	1.097	−0.681	−0.623	0.167	0.165
Lab C (70601W_DD)	25.5	0.687	1.087	1.125	−0.759	−0.684	0.182	0.182

H: horizontal; V: vertical.

Table 5. Spatial void distance results for Gel push and reconstituted samples – small particles less than 75 μm ('Fines') removed from images.

			Mean log spacing		Kurtosis		Dispersion	
Sample	Image 'Fines' removed (%)	Void ratio	V	H	V	H	V	H
Gel Push-A	5.4	0.827	1.380	1.429	−0.534	−0.460	0.183	0.183
Gel Push-B	52.8	2.191	1.701	1.742	−0.437	−0.437	0.208	0.224
Lab C (40601H_DD)	20.4	1.248	1.492	1.499	−0.321	−0.202	0.175	0.176
Lab C (40601W_DD)	17.4	1.188	1.477	1.523	−0.331	−0.276	0.181	0.184
Lab C (70601H_DD)	28.3	1.174	1.523	1.569	−0.267	−0.168	0.167	0.164
Lab C (70601W_DD)	25.5	1.132	1.473	1.512	−0.325	−0.378	0.177	0.181

The determined distribution of particle spacing gave a highly positive-skewed void distribution as seen previously (Bowman & Soga, 2003). Hence, the log of the void spacing was used to produce a near-normal distribution upon which statistical analysis could be performed. Table 4 presents spatial void distance results for gel push and reconstituted samples for all particles while Table 5 presents the same data with the 'fines' removed (i.e. particles <75 μm). Averaged data across all images taken for each test are given for all results including mean log spacing, index of dispersion and kurtosis. Effective void ratio is also reported in these tables – Table 5 highlights how fines removal results in a large increase in the void ratio determined by image processing. In order to examine the results considering local density effects, data from the individual images (nine for each test) are separately presented in the following analysis against the mean void ratio of each image.

Mean log spacing against void ratio

As shown in Table 4, both gel push and dry deposition samples generally have smaller void distances in the vertical direction than in the horizontal due to the horizontally orientated fabric (Masad, 1998). Plots of mean void distance against void ratio for the gel push and reconstituted samples are shown in Figures 10 and 11, respectively. Here we see that Gel Push-A, a relatively clean sand, has a narrow range of void ratios across the images, while Gel Push-B, with a much greater degree of fines, has a much wider range. The populations are also quite distinct, with Gel Push-B plotting at much lower values than Gel Push-A due to the larger quantity of fines reducing the void distance at the same void ratio. In Figure 11, the two populations of images taken for the loose and dense samples plot adjacent to each other in terms of void ratio (indicated by the ovals), irrespective of ageing. However, they overlap considerably in terms of mean log mean spacing (Table 4) and there is much greater variation within the populations than for the gel push samples. The likelihood is that the particle populations in which spacing is large (e.g. in 70601W_DD) are dominated by greater numbers of large particles than usual, that is,

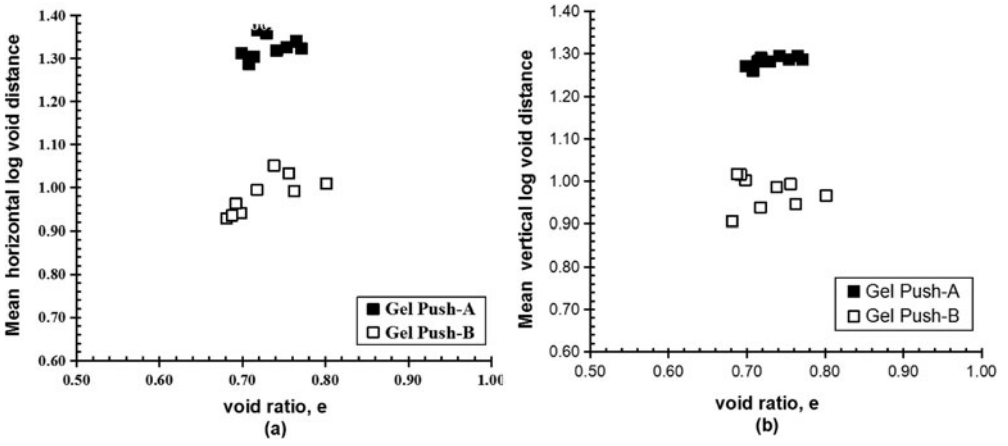

Figure 10. Mean log void distance for Gel Push-A and Gel Push-B (a) horizontal (b) vertical.

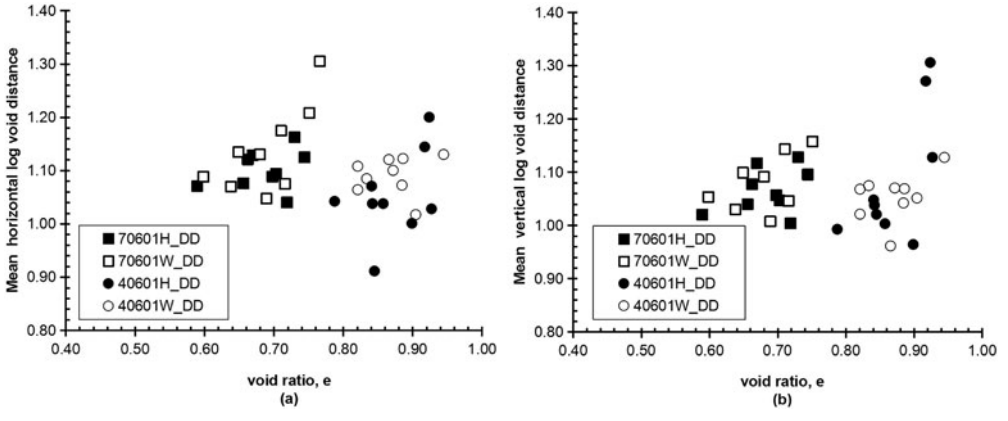

Figure 11. Mean log void distance of all particles for reconstituted samples (a) horizontal and (b) vertical.

images taken do not contain so many fines. When this occurs the void ratio can be the same, but the mean distance is increased. This segregation of particles is evident in Figure 7(b,c).

With respect to the influence of duration of loading on particle spacing, based on all particles, Table 4 and Figure 11 show no clear trends between one-hour and one-week samples. However, as the fines content for these samples is 15%, below the transition fines content of this material (see Figure 1(b)), the overall behaviour is expected to be sand dominated. Thus, further image analysis was carried out using sand-sized particles only.

Figure 12 present the mean log void distance relationships for sand-sized particles only for dense and loose samples, respectively. For dense samples, statistical examination shows that there are strong correlations, horizontally and vertically, between void ratio and mean log spacing, for one hour and one week. For loose samples, while the trend is similar, the correlation is reduced as a result of its fabric being more variable (Jang & Frost, 1998). The close relationship between void ratio and spacing upon removal of the fines also highlights the dominant role that the sand-sized particles play at this fines content.

Kurtosis against void ratio

Figure 13 plots kurtosis of the log mean spacing versus void ratio for dense and loose reconstituted samples. The relationships seen are relatively weak although some trends can be observed. For loose samples, kurtosis tends to decrease (become more negative) with time under load

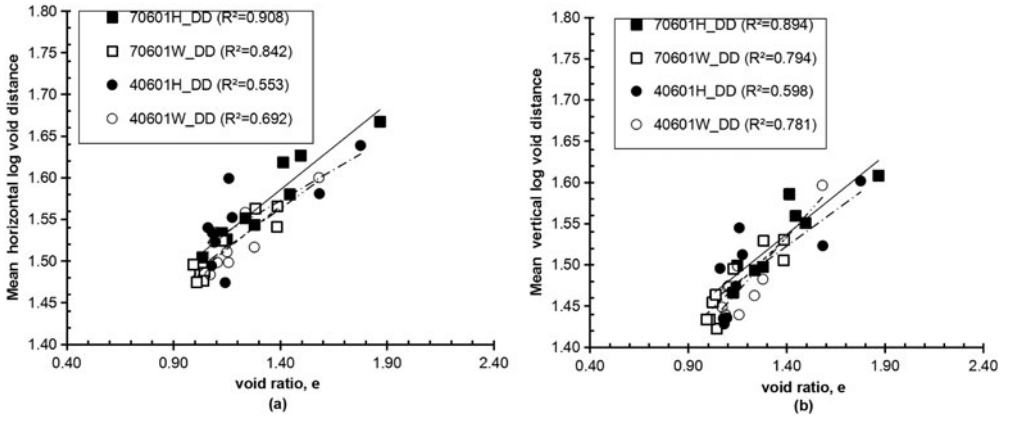

Figure 12. Mean log void distance for reconstituted samples (sand-size only) (a) horizontal and (b) vertical.

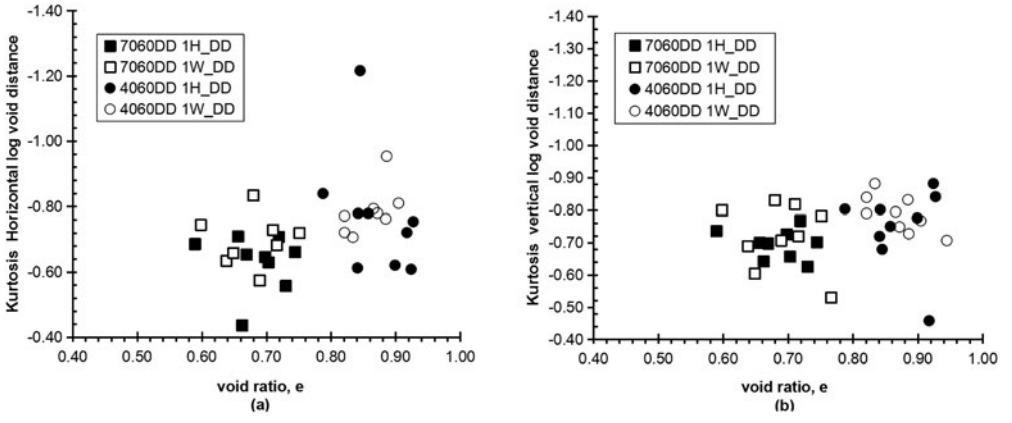

Figure 13. Kurtosis of log void distance of all particles for reconstituted samples: (a) horizontal and (b) vertical.

vertically, that is, from –0.745 to –0.787 while in the horizontal direction, kurtosis increases, that is, from –0.770 to –0.699. For dense samples, the kurtosis reduces with time, that is, from –0.681 to –0.759, vertically, and from –0.623 to –0.684, horizontally. Considering the sand-sized particles only, both dense and loose samples also show that kurtosis becomes lower with time, as can been seen in Figure 14 and Table 5.

While there is no systematic difference between Gel Push-A and B samples with respect to kurtosis (Table 4 and Figure 15), comparing these with the Lab C samples (Figures 13 and 14) we see both Gel Push-A and B generally have higher (less negative) kurtosis values – however, when fines are removed via image analysis (which increases the kurtosis values in all cases) the values do not change as much as for Lab C. It is particularly notable that, despite the large quantity of fines present, the kurtosis for Gel Push-B does not shift as much in the positive direction as the others. This may be because this sample had a large portion of its fines below 32 μm (which were removed for the Lab C tests) – in which case kurtosis is shown to be very sensitive to both the fines size and its proportion. This means that while kurtosis can show changes due to age within soils of a particular PSD, it may not be appropriated to compare between soils of differing PSD.

Index of dispersion against void ratio

Figure 16 and Table 4 show index of dispersion versus void ratio. For the dense reconstituted samples, the index of dispersion from one hour to one week increases both in the vertical (from

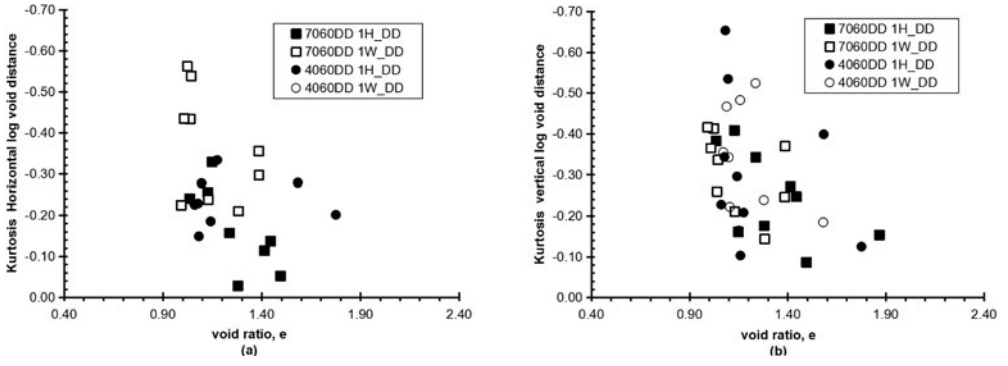

Figure 14. Kurtosis of log void distance (sand-sized particles only), for reconstituted samples (a) horizontal direction and (b) vertical.

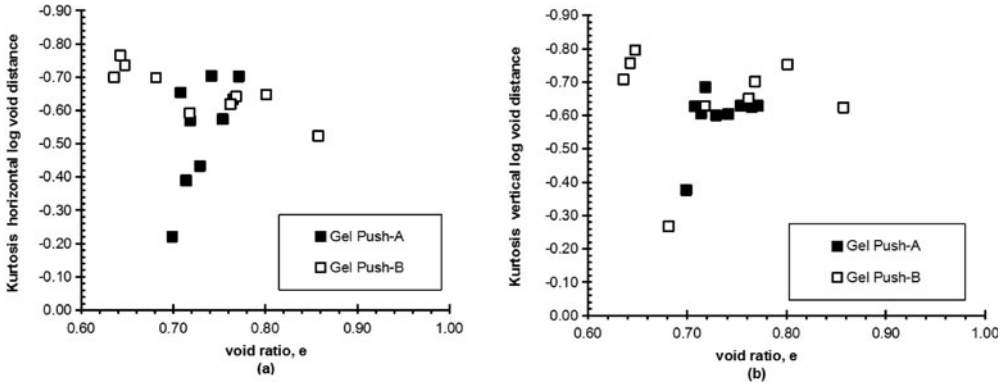

Figure 15. Kurtosis of log void distance for undisturbed samples Gel Push-A and Gel Push-B (a) horizontal direction and (b) vertical.

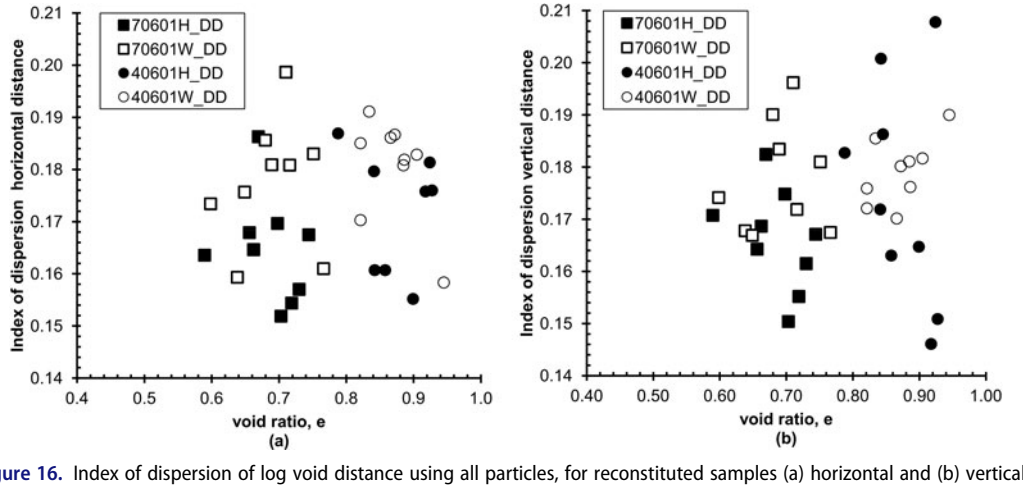

Figure 16. Index of dispersion of log void distance using all particles, for reconstituted samples (a) horizontal and (b) vertical.

0.167 to 0.177) and horizontal directions (from 0.164 to 0.181). A similar tendency for dispersion to increase also applies to sand-sized only particles (Figure 17 and Table 5). For loose samples, Table 4 shows that the index of dispersion tends to increase with time but to a lesser degree, that is, 0.179 to 0.186 (vertical) and 0.173 to 0.174 (horizontal) from one hour to one week. Sand-sized only particles also show the same tendency, with Figure 17 giving a clearer indication

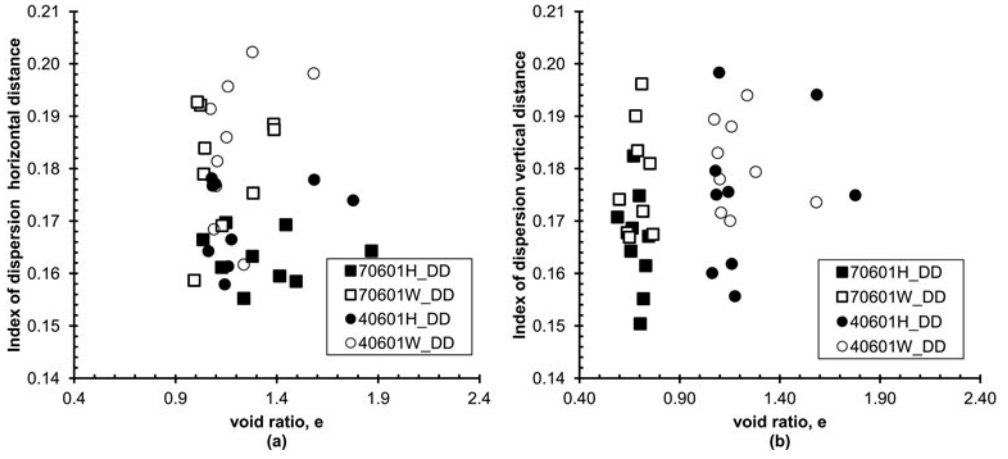

Figure 17. Index of dispersion of log void distance (sand-sized particles only) for reconstituted samples (a) horizontal and (b) vertical.

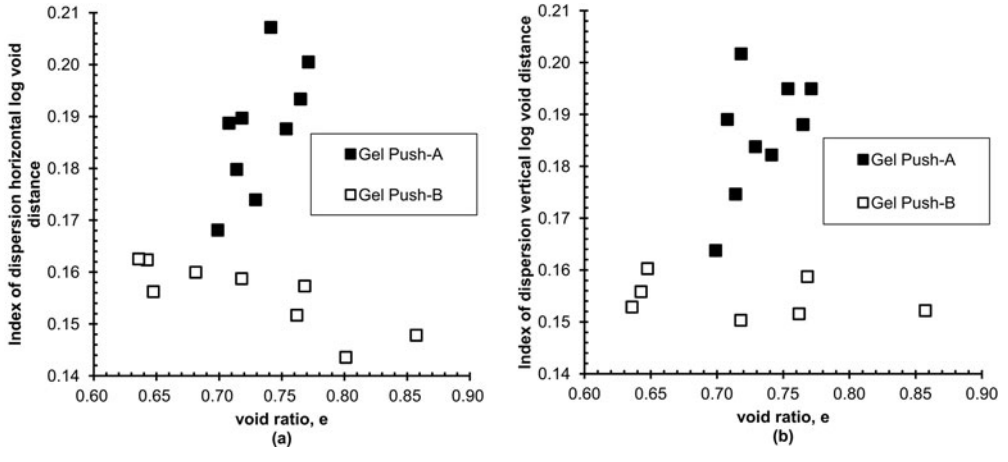

Figure 18. Index of dispersion of log void distance for undisturbed samples Gel Push-A and Gel Push-B (a) horizontal and (b) vertical.

than examining Table 5 alone. We see that changes in spatial dispersion for dense samples with time tend to be larger than that for loose samples, which is keeping with the findings of previous researchers (e.g. Baxter & Mitchell, 2004; Bowman, 2002) who noted that the ageing effect is more profound in dense than in loose materials.

Regarding the undisturbed samples (Figure 18), the index of dispersion of Gel Push-A is larger than Gel Push-B, which may be related to the different dominant particle sizes (noting that A has considerably fewer fines than B). The index of dispersion of reconstituted samples also tends to lie between Gel Push-B and A, which supports the idea that fines content (which is intermediate), plays a role, although the dispersion measure is meant to enable populations with different means to be directly compared. Further analysis of this measure is needed to enable population comparisons of different particle sizes to be more directly made.

The lack of a distinct difference between the gel push and reconstituted samples suggests that the undisturbed samples in this study are little structured. This is not altogether surprising considering that large strains will have been applied to the soil during the main earthquake shocks on 4 September 2010 (Darfield Earthquake, Mw 7.1) and 22 February 2011 (Canterbury Earthquake, Mw 6.3, which caused liquefaction at the site) – as shown schematically in Figure 19.

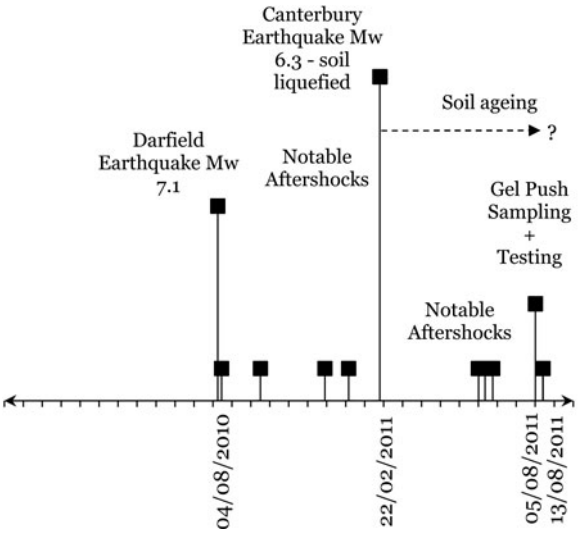

Figure 19. Timeline of key influences of ageing of the Gel Push samples.

The soil also continued to be disturbed during the many aftershocks that occurred until sampling, with a notable aftershock series (Mw 6.3) occurring on 13 June 2011. In addition, although care was taken to minimise the disturbance during the sampling (on 5 August 2011), transportation, laboratory handling and final testing (on 13 August 2011), some degree of disturbance may have occurred. Taylor et al. (2012) evaluated the quality of gel push samples by comparing the shear wave velocity from the laboratory (bender element test) and from field tests (downhole seismic test). The comparison showed close agreement between them, indicating high sample quality. However, when the laboratory data were normalised by the field data, they reported that undesirable strain may still be induced in samples taken. From this, it seems that time 'zero' at which aging would commence can be taken, at the earliest, from the date of the Canterbury Earthquake when the site was liquefied but could be as late as the date of sampling.

Conclusions

Methods and challenges in quantifying the microstructure of sand containing fines and time-dependent microstructural changes have been described. Based on circular statistical analysis, it is seen that the microstructure of undisturbed natural silty sands and dry deposition silty sand samples have a very similar preferred horizontal orientation, as expected. Parameters previously used for clean sands to statistically measure particle spatial relationships, namely mean log spacing, variance and kurtosis were rigorously examined for their application to silty sands. In doing so, a new parameter, index of dispersion (variance to mean ratio) applied to the spacing distribution was found to be better than kurtosis to unambiguously indicate a more interlocked structure, thus a more aged sample according to the theory of mechanical interlock. As determined by the index of dispersion increasing with age, the loading of reconstituted samples under K_0 condition resulted in particles clustering together over time up to a week, with this trend being greater in dense than in loose soil. This may be due to void collapse in loose soil dominating creep behaviour, in contrast to particle clustering via void growth dominating in dense soil. This behaviour reflects similar findings from the field that indicates granular soil ageing to be greater in dense than in loose soil.

It was seen that it may be difficult to directly apply the index of dispersion measure to compare the ages of samples of different PSD. That is, the values found for the reconstituted samples, which had an intermediate level of fines (15%), tended to lie between that of Gel Push-B

(35%) and Gel Push-A (4%) field samples of the same age. This means that dispersion is influenced by the PSD, albeit in a systematic manner. Hence, further work is needed to identify how this parameter or a combination of parameters can be developed to enable such comparisons to be directly made

Acknowledgements

The authors would like to thank the following University of Canterbury technicians: Messers Siale Faitotonu (Geomechanics), Mike Flaws (Electron Microscopy), John Koolos (Transportation) and Rob Spiers (Geological Sciences).

Disclosure statement

No potential conflict of interest was reported by the authors.

Funding

The first author was supported by Postgraduate Scholarship 146/D4.4/PK from the Directorate General of Higher Education, Ministry of Education and Culture of Indonesia, while New Zealand Earthquake Commission (EQC) Capability Funding is also gratefully acknowledged.

References

Ashford, S. A., Rollins, K. M., & Lane, J. D. (2004). Blast-induced liquefaction for full-scale foundation testing. *Journal of Geotechnical and Geoenvironmental Engineering*, *130*(8), 798–806.

Astedt, B., Weiner, L., & Holm, G. (1992). Increase in bearing capacity with time for friction piles in silt and sand. *Proceeding of Nordic Geotechnical Meeting*, 411–416.

Baxter, C. D. P., & Mitchell, J. K. (2004). Experimental study on the aging of sands. *Journal of Geotechnical and Geoenvironmental Engineering*, *130*(10), 1051–1062.

Bowman, E. T. (2002). *The Ageing and creep of dense granular material* (Doctoral dissertation). University of Cambridge, Cambridge, UK. Available from ProQuest Dissertations & Theses A&I (U169772).

Bowman, E. T., & Soga, K. (2003). Creep, ageing and microstructural change in dense granular materials. *Soils & Foundations*, *43*(4), 107–117.

Bullock, P. J., Schmertmann, J. H., McVay, M. C., & Townsend, F. C. (2005). Side shear setup. II: Results from Florida test piles. *Journal of Geotechnical and Geoenvironmental Engineering*, *131*(3), 301–310.

Chatfield, C. (1983). *Statistic for technology* (3rd ed.). London: Chapman and Hall.

Cubrinovski, M. (2013). Liquefaction-induced damage in 2010-2011 Christchurch (New Zealand) earthquakes. Proceeding of 7th International Conference on Case Histories in Geotechnical Engineering, Chicago, IL.

Cubrinovski, M., Hughes, M., Bradley, B., McCahon, I., McDonald, Y., Simpson, H., … O'Rourke, T. (2011). Liquefaction impact on pipe networks. Retrieved from University of Canterbury Research Repository website https://ir.canterbury.ac.nz/handle/10092/10178

Cubrinovski, M., & Ishihara, K. (2002). Maximum and minimum void ratio characteristic of sands. *Soils & Foundations*, *42*(6), 65–78.

Fisher, N. I. (1993). *Statistical analysis of circular data*. Cambridge: Cambridge University Press.

Hoeg, K., Dyvik, R., & Sandbaekken, G. (2000). Strength of undisturbed versus reconstituted silt and silty sand specimens. *Journal of Geotechnical and Geoenvironmental Engineering*, *126*(7), 606–617.

Huang, A. B., Tai, Y. Y., Lee, W. F., & Ishihara, K. (2008). Sampling and field characterization of the silty sand in Central and Southern Taiwan. 3rd International Conference on Site Characterization, Taipei.

Japanese Geotechnical Society. (2009). JGS 0161: Test method for minimum and maximum densities of sands. JGS, Japan.

Jang, D. J. (1997). *Quantification of sand structure and its evolution during shear using image analysis* (Doctoral dissertation). Georgia Institute of Technology. Retrieved from ProQuest Dissertations & Theses A&I (9735904).

Jang, D. J., & Frost, J. D. (1998). Sand structures differences resulting from specimen preparation procedures. ASCE Specialty Conference on Geotechnical Earthquake Engineering and Soil Dynamic, Seattle.

Johnson, M. E., Tietjen, G. L., & Beckman, R. J. (1980). A new family of probability distributions with applications to Monte Carlo studies. *Journal of the American Statistical Association*, *75*(370), 276–279.

Kang, D. H., Yun, T. S., Lau, Y. M., & Wang, Y. H. (2012). DEM simulation on soil creep and associated evolution of pore characteristics. *Computers and Geotechnics*, *39*, 98–106.

Kazuo, T., & Kaneko, S. (2006). Undisturbed sampling method using thick water-soluble polymer solution Tsuchi-to-Kiso. *Journal of the Japanese Geotechnical Society*, *54*(4), 145–114.

Kuo, C. Y., Frost, J. D., & Chameau, J.-L. A. (1998). Image analysis determination of stereology based fabric tensors. *Géotechnique*, *48*(4), 515–525.

Lade, P. V., Liggio, J., & Yamamuro, J. A. (1998). Effect of non-plastic fines on minimum and maximum on void ratios of sand. *Geotechnical Testing Journal*, *21*, 336–347.

Lloyd, G. (1987). Atomic number and chrystallographic contrast images with the SEM: A review of backscattered electron techniques. *Mineralogical Magazine*, *51*, 3–19.

Masad, E. (1998). *Permeability simulation of reconstructed anisotropic soil medium* (Doctoral dissertation). Washington State University. Retrieved from ProQuest Dissertations & Theses A&I (9917441).

Masad, E., & Muhunthan, B. (2000). Three dimensional characterization and simulation of anisotropic soil fabric. *Journal of Geotechnical and Geoenvironmental Engineering. ASCE*, *126*(3), 199–207.

Mitchell, J. K., & Soga, K. (2005). *Fundamentals of soil behaviour* (3rd ed.). Hoboken, NJ: John Wiley & Sons.

Muszynski, M. R. (2000). *Void ratio distribution of normally consolidated coarse-grain magnetic tailings as a function of aging time* (Unpublished master's thesis). Michigan Technological University, Houghton, MI.

Ng, W. K., Selamat, M. R., & Choong, K. K. (2010). Soil/pile set-up effects on driven pile in Malaysian soil. *Electronic Journal of Geotechnical Engineering*, 15A, 1–12.

Oda, M., & Iwashita, K. (1999). *Introduction to mechanics of granular materials*. Rotherdam, The Netherland: Balkema.

Palmer, S. N., & Barton, M. E. (1986). Avoiding microfabric disruption during the impregnation of friable uncemented sands with dyed epoxy. *Sedimentary Research*, *56*, 556–557.

Saftner, D. A. (2009). Sand aging: Time dependent strength gain in recently disturbed sand. Proceedings of the 4th International Young Geotechnical Engineer's Conference, Alexandria, Egypt.

Stringer, M. E., Cubrinovski, M., & Haycock, I. (2016). Experience with gel-push sampling in New Zealand. Proceeding of 5th International Conference on Site Characterization, Gold Coast Australia.

Taylor, M. L., Cubrinovski, M., & Haycock, I. (2012). Application of new 'Gel-push' sampling procedure to obtain high quality laboratory test data for advanced geotechnical analyses. Proceeding of 12th NZSEE Conference, Christchurch, New Zealand.

Vlahinić, I., Andò, E., Viggiani, G., & Andrade, J. (2014). Towards a more accurate characterization of granular media: Extracting quantitative descriptors from tomographic images. *Granular Matter*, *16*(1), 9–21.

Yamamuro, J. A., & Wood, F. M. (2004). Effect of depositional method on the undrained behavior and microstructure of sand with silt. *Soil Dynamics and Earthquake Engineering*, *24*(9–10), 751–760.

Yamamuro, J. A., Wood, F. M., & Lade, P. V. (2008). Effect of depositional method on the microstructure of silty sand. *Canadian Geotechnical Journal*, *45*(11), 1538–1555.

Yang, C. T. (2002). *Boundary condition and inherent stratigraphic effects on microstructure evolution on sand specimens* (Doctoral dissertation). Georgia Institute of Technology. Retrieved from ProQuest Dissertations & Theses A&I (3046948).

Yusa, M. (2015). *Aging and creep of silty sand* (Doctoral dissertation). Retrieved from https://ir.canterbury.ac.nz/handle/10092/10754

Yusa, M., & Bowman, E. T. (2013). Quantification of time-dependent microstructural change of a silty sand under load. Powders and Grains 2013, Sydney.

Yusa, M., Bowman, E. T., & Cubrinovski, M. (2017). Observation of microstructure of silty sand obtained from gel push sampler and reconstituted sample. EPJ Web Conference, 140, 12017.